SERBIAN JOURNAL OF ELECTRICAL ENGINEERING
Vol. 21, No. 1, February 2024, 1-37
UDC: 621.316.1:621.33-835 **DOI: https://doi.org/10.2298/SJEE2401001P**

Cheetah Optimization Algorithm for Simultaneous Optimal Network Reconfiguration and Allocation of DG and DSTATCOM with Electric Vehicle Charging Station

Arvind Pratap[1], Prabhakar Tiwari[1], Rakesh Maurya[2], Bindeshwar Singh[3]

Abstract: The potential of Electric Vehicles (EVs) to decarbonize the transportation industry has attracted a lot of attention in recent years in response to growing environmental concerns. Electric Vehicle Charging Stations (EVCSs) need to be properly located for widespread EV integration. The distribution system is facing additional challenges due to inclusion of EVCS. The adverse impacts of EVCS on the Radial Distribution Network (RDN) may be minimized using Distributed Generations (DGs) or Distribution Static Compensators (DSTATCOMs) or by reconfiguring the network. This paper uses a novel optimization technique to solve the problem of simultaneous optimal placement of EVCS with network reconfiguration and optimal planning (siting and sizing) of DGs and DSTATCOMs. The multiple objective functions are considered in order to minimize the active power losses, the voltage deviation, the investment costs for DGs and DSTATCOMs, and to increase the voltage stability of the system. A novel meta-heuristic Cheetah Optimization Algorithm (COA) is used to solve the optimization problem. To examine the effectiveness of the suggested strategy on 33-bus and 136-bus networks, several scenarios of simultaneous incorporation of EVCS, DG, and DSTATCOM installations with network reconfiguration are taken into consideration. The COA results are also compared to the results of grey wolf optimization and genetic algorithms.

Keywords: Network Reconfiguration, Distributed Generation, Electric Vehicle charging Station, Real Power Loss reduction, Distribution Static Compensator.

[1] Madan Mohan Malaviya University of Technology, Department of Electrical Engineering, Gorakhpur, UP, India; E-mails: arvind.pratap366@gmail.com; tiwarip6@gmail.com
[2] Sardar Vallabhbhai National Institute of Technology, Department of Electrical Engineering, Surat, India; E-mail: rmaurya@eed.svnit.ac.in,
[3]Kamla Nehru Institute of Technology, Department of Electrical Engineering, Sultanpur, India; E-mail: bindeshwar.singh2025@gmail.com

Abbreviations

CB	Capacitor Banks
COA	Cheetah Optimization Algorithm
GOA	Grasshopper Optimization Algorithm
GWO	Grey Wolf Optimizer
ICRI	Investment Cost Reduction Index
IRPL	Real Power Loss Index
ITVD	Index for Total Voltage Deviation
MOF	Multi Objective Function
NR	Network Reconfiguration
PSO	Particle Swarm Optimization
RPL	Real Power Loss
VD	Voltage Deviation
VP	Volage Profile
VS	Voltage Stability
VSI	Voltage Stability Index
WNR	With Network configuration
WONR	Without Network configuration

Symbols

α	DG unit's rate of return on capital investment
br	Total branches in network
C_{dg} , C_{dst}	Capital cost of DG [$/kW] and DSTATCOM [$/kVAr]
d, n	Dimension of the search space and population size
N_{bus}	Total nodes in network
N_{dst} , N_{dg}	Total number of DSTATCOM and DG units
N_D , N_S	DG and DSTATCOM life spans in years
P_j , P_k	Effective active power load at j and k bus
P_{loss}^{bc} , P_{loss}^{wc}	Real power losses with initial condition and different cases
P_{ss}	Real power supplied by feeder
P_{cs}	Total real power demand by EVCSs
$P_{dg,\max}^{k}$, $P_{dg,\min}^{k}$	Maximum and minimum real power injection limits of DG
$P_{dg,i}$	Real power drawn from i^{th} DG unit
P_{load}	Total real power load demand of the system
Q_{load}	Total reactive power load demand of the system
Q_j , Q_k	Effective reactive power load at j and k bus
Q_{loss}	Reactive power loss
$Q_{dst,\min}^{k}$, $Q_{dst,\max}^{k}$	Minimum and maximum reactive power injection limits of DSTATCOM

$Q_{dst,i}$	Reactive power injected by i^{th} DSTATCOM
Q_{ss}	Reactive power provided by feeder
R_{jk} , X_{jk}	Resistance and reactance of *jk*-branch
V_k^{wc} , V_k^{bc}	Voltage of k^{th} bus with different cases and initial condition
V_j , V_k	Voltage of j^{th} and k^{th} bus
$V_{\min}$	Minimum bus voltage in p.u.
ν	DSTATCOM's asset rate of return

1 Introduction

One of the major sources of air pollution and greenhouse gas emissions is the utilization of automobiles driven by internal combustion engines. In such a scenario, Electric Vehicles (EVs) can play an important role in the decarbonization of the transportation sector. However, the load demand on the distribution side has increased due to a new class of electric loads. Furthermore, it results in additional power loss and voltage fluctuations in the distribution network. Researchers have focused more emphasis on EVCS to accommodate the rising demand for EVs throughout the world. Integration of renewable Distributed Generation (DG) technologies into distribution networks has the potential to significantly improve system performance. Additionally, Distribution Static Compensator (DSTATCOM) is also utilized to resolve issues associated with power quality in distribution networks, such as excessive power loss and voltage instability. The negative impact of EV Charging Station (EVCS) on RDN can be reduced by the incorporation of the intelligent alternative scheduling option provided by the combination of renewable DG technology and DSTATCOM in the RDN. Several technical and economic advantages may be achieved by integrating DGs and DSTATCOM with EVCS in distribution systems at the same time. Furthermore, the optimal device allocation is crucial for maximizing technical and economic benefits. Numerous metaheuristic optimization strategies had been used by researchers to ascertain the optimal location of EVCS in coordination with optimal planning (siting and sizing) of DG and DSTATCOM units on the RDN.

The authors of [1] proposed a chaotic student psychology-based optimization (CSPBO) method to determine the optimal site and size of DG units to mitigate the detrimental impact of EVCS on the RDNs. In [2], the authors employed a Transient Search Optimization (TSO) algorithm for optimal allocation of EVCS with DG on 25-bus unbalanced RDN with goals of improving the VP and minimizing the RPL. In [3], the authors presented a hybridized GWO and PSO (HGWOPSO) algorithm for optimal allocation of DG in order to mitigate the detrimental impact of EVCS on the RDN. In addition to this, multiple objective

functions are considered to minimize the RPL, VD, and VSI reduction for optimal allocation of DG to enhance the performance of the EVCS-loaded RDN. In [4], the authors proposed a methodology to determine the optimal placement and capacity of EVCS in an unbalanced RDN using PSO algorithm. Furthermore, the goal of the research is to mitigate the negative effects of EVCS by strategically placing extra DGs units on an unbalanced RDN. The study also examined the impact of EVCS deployment on the RPL and VP of the system. In [5], the authors employed Genetic Algorithm (GA) for simultaneous optimal planning (placing and sizing) of EVCSs and DGs by optimizing multiple objectives such as investment costs, system reliability, RPL, VP, and environmental benefits on the RDN. In [6], the authors employed the Arithmetic Optimization (AO) algorithm for the optimal allocation of DG units with EVCS to minimize RPL on the RDN. The authors of [7] presented a method for optimal planning of different types of DG units to mitigate negative impact of EVCS on the RDN. In addition to this, Harries Hawk Optimization (HHO) and Teaching-Learning Based Optimization (TLBO)algorithms were used to minimize the RPL, VD and VSI reduction for optimal planning of DG with EVCS on RDNs.

The authors of [8] used the Marine Predators' Algorithm (MPA) for optimum allocation of DG and CB with EVs to reduce RPL and enhance the VSI of an 83-bus Taiwan distribution system. In [9], a two-stage GOA-based fuzzy multi-objective scheme was employed for optimal planning of DG, CB, and EVCSs on the RDNs. The proposed algorithm was used in the first stage to determine the optimal site and size of DGs and CB to improve system power factor, VP and minimize the RPL, while the optimal sites and sizes of EVCS on the distribution system connected with DGs and CB were determined in the second stage. The authors of [10] used the HGWOPSO algorithm for optimum allocation of EVCS with CB on the RDNs to lessen the negative impacts of EVCS on the RDNs with the aims of minimizing the RPL, maximizing the net profit, and improving the system's reliability. In [11], the authors employed the African Vulture Optimization (AVO) algorithm for simultaneous optimal placement of EVCS with allocation of DG and DSTATCOM units on the RDN. The primary objective was to minimize RPL, VD, and VSI reductions in the distribution system. However, the economic aspects for the installation of DG and DSTATCOM units and the significance of NR were not addressed in this study. The authors of [12] employed a Cooperative Spiral GA with Differential Evolution (CoSGADE) algorithm for the optimal allocation of EVCS with DG and CB units to minimize RPL, VD, and VSI reduction of 15, 69, and 118-bus RDNs.

In [13], the authors proposed a hybridized AVO and Pattern Search (HAVOPS) algorithm for optimal planning of DG and DSTATCOM with NR to minimize the RPL and VD while maximizing the VSI of the EVCS loaded RDN. However, the simultaneous approach for optimum placement of EVCS with DG, DSTATCOM, and NR was not considered. The authors of [14] employed the

PSO algorithm for optimal planning of EVCS with DG and NR in order to minimize the investment and loss costs of an imbalanced RDN. The authors of [15] used a hybridized Bacterial Foraging Optimization and PSO (HBFOPSO) algorithm for optimal allocation of EVCS with photovoltaic-based DG system on RDN in order to minimize RPL, VD, and VSI reduction. In [16], the authors used the Honey Badger Algorithm (HBA) to tackle the issue of simultaneous optimum NR and DG allocation, with the goal of lowering RPL, boosting the system's VP, and minimizing greenhouse gas emissions while taking EV load penetration into consideration. In order to address NR issues, the authors of [17] presented a framework for incorporating radiality constraints into mathematical models of optimization problems for RDN. The authors of [18] used a Harmonic Search Algorithm (HSA) to solve the NR issue in the presence of DG units with the objective of minimizing the RPL and enhancing the VP of the RDNs at different load levels. The authors of [19] suggested a cooperative coevolutionary GA method for simultaneous fast charging station allocation and NR with the goal of minimizing investment and energy loss costs.

Table 1

Taxonomy of previous related works and the author's contribution.

Reference	DG	DSTATCOM/ CB	NR	Simultaneous incorporation of EVCS, DG, DSTATCOM & NR	Techniques	Objectives			
						Investment Cost of DG / DSTATCOM	RPL	VD	VSI
[1]	√	×	×	×	CSPBO	√	√	√	×
[3]	√	×	×	×	HGWOPSO	×	√	√	√
[4]	√	×	×	×	PSO	×	√	√	×
[6]	√	×	×	×	AO algorithm	×	√	×	×
[7]	√	×	×	×	HHO and TLBO	×	√	√	√
[8]	√	×	×	×	MPA	×	√	×	√
[11]	√	√	×	×	AVO algorithm	×	√	√	√
[12]	√	√	×	×	CoSGADE	×	√	√	√
[13]	√	√	√	×	HAVOPS	√	√	√	√
[14]	√	×	√	×	PSO	√	√	×	×
[15]	√	×	×	×	HBFOPSO	×	√	√	√
[20]	√	×	√	×	Unified PSO	×	√	×	×
[21]	√	×	×	×	GOA	×	√	×	×
[22]	√	×	×	×	Simulated annealing with PSO	×	√	√	×
[23]	√	√	√	√	Bat algorithm	×	√	×	×
This paper	√	√	√	√	COA	√	√	√	√

The aforementioned literature describes a number of heuristic and meta-heuristic approaches for optimal placement of EVCS with different compensating devices. In addition, a MOF considering RPL, VD, and VSI is used in most work. As far as the authors are aware, this is the first time that COA [24], a nature-inspired algorithm inspired by the hunting techniques of cheetahs, has been applied to the problem of maximizing the technical and economic benefits by achieving simultaneous optimal placement of EVCS with optimal NR and planning (siting and size) of DG and DSTATCOM units on RDN. Furthermore, **Table 1** shows that very few research has been conducted on the economic aspects and simultaneous planning of EVCS, DG, and DSTATCOM with optimal NR. The main contributions to this article are as follows:

- Simultaneous optimal placement of EVCS in coordination with optimal NR and planning (siting and sizing) of DGs and DSTATCOMs.
- A MOF is formulated, considering technical factors such as reducing IRPL and ITVD while maximizing VSI, along with economic aspects related to investment costs for DG and DSTATCOM.
- The computational efficiency of the COA is examined on the 136-bus network [25], which is a real part of Brazil's Tres Lagoas distribution system.
- COA's computational efficiency is compared to GWO's [26] and GA's [27].

The subsequent sections of this paper are structured as follows: The mathematical problem formulation is discussed in Section 2. The overview and implementation of the COA on the specified optimization problem are discussed in Section 3. The simulation findings, which include a comparison to GWO and GA, are reported in Section 4, while Section 5 summarizes the research results.

2 Mathematical Problem Formulations

The aim of this section is to develop a multi-objective optimization problem that includes the optimal NR and allocation of multiple EVCS, DG, and DSTATCOM units with the aim of minimizing several adopted objective functions. In this work, the EVCS is modelled as a sink that absorbs the system's actual power during EV battery charging [28], while the DG and DSTATCOM are modelled as active and reactive power sources, respectively, and operate under steady-state conditions. The mathematical modelling of EVCS is based on the work presented in [11, 13, 28], while the DG and DSTATCOM modelling is based on the work presented in [11, 13] and [29]. A hypothetical RDN with a branch *jk* between buses *j* and *k* is depicted in Fig. 1. The NR modelling, MOF, and system constraints are discussed in Subsections 2.1–2.7, subsequently.

2.1 Network reconfiguration

The process of reconfiguring a network involves opening the sectionalizing switches and closing the tie switches [18, 30]. This switching is carried out such

that the network's radial topology is preserved and all loads are powered on. The optimal reconfiguration issue involves disconnecting or rerouting feeders to reduce power losses. A severely loaded line may be relieved by rearranging the distribution system. In this work, the optimal reconfiguration of the distribution network is determined using COA. After identifying the fundamental loops in the network using graph theory, the Bus Incidence Matrix (BIM) is computed. If the determinant of BIM [30] is 1 or -1, then the radial topology continues to hold; otherwise, the next possible solution is investigated using COA. The Total Fundamental Loop (TFL) in a RDN can be determined using (1).

$$TFL = br - (N_{bus} - 1). \tag{1}$$

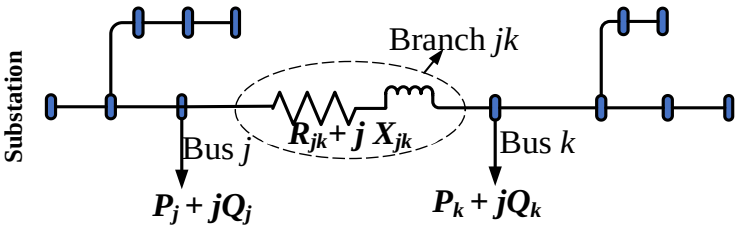

Fig. 1 – *Hypothetical radial distribution network.*

2.2 Formulation of weighting factors based multi-objective functions

In this paper, three performance indices (IRPL, ITVD, and VSI) are taken into account for enhancing the technical advantages of the RDN and one performance index (ICRI) for reducing the investment costs associated with installing the DG and DSTATCOM units [31]. In addition to this, the weighting factors are used to formulate the multiple objective functions in a single mathematical equation [32], as given by (2). In this work, the decision variables in the optimization problem are the location of EVCS, switches to be opened for optimal NR, and locations of compensating devices along with their optimal sizes. Furthermore, the decision variables are optimized to achieve the minimization of multiple objective functions.

$$MOF = \min\left\{\beta_1 \times J_1 + \beta_2 \times J_2 + \beta_3 \times J_3 + \beta_4 \times J_4\right\}, \tag{2}$$

where β_1, β_2, β_3 and β_4 are the weighting factors associated with J_1, J_2, J_3 and J_4, respectively. The sum of all the weighting factors must be equal to one. The various adopted objective functions (J_1, J_2, J_3, J_4) are discussed in Subsections 2.3–2.6, subsequently.

2.3 Minimization of IRPL (J_1)

The first objective function J_1 is utilized to minimize the RPL of the network by minimizing the value of IRPL while satisfying the system constraints [13]. Mathematically, J_1 can be defined as:

$$J_1 = Minimize\left(IRPL\right). \tag{3}$$

The IRPL for the RDN can be formulated as the ratio of the actual power loss at different cases to the power loss at base case [33], and which can be expressed as provided by (4). The real power loss in the branch *jk* can be computed using (5):

$$IRPL = \frac{P_{loss}^{wc}}{P_{loss}^{bc}}, \tag{4}$$

$$P_{ll}\left(jk\right) = \frac{\left(P_k^{\,2} + Q_k^{\,2}\right)}{V_k^{\,2}} R_{\,jk}\,. \tag{5}$$

The total real power loss of the network can be calculated as the sum of power losses in all branches using (6).

$$P_{loss} = \sum_{jk=1}^{br} P_{ll}\left(jk\right), \tag{6}$$

where P_{loss} denotes total active power loss in the RDN and P_{ll} denotes active power loss in *jk* branch.

2.4 Minimization of ITVD (J_2)

The second objective function J_2 is utilized to improve the VP of buses in the RDN by minimizing the value of the ITVD while satisfying the system constraints [13, 34]. Mathematically, J_2 can be defined as:

$$J_2 = Minimize\left(ITVD\right). \tag{7}$$

The ITVD for the RDN can be expressed as provided by (8):

$$ITVD = \frac{\sum_{k=1}^{N_{bus}} \left(1 - V_k^{wc}\right)}{\sum_{k=1}^{N_{bus}} \left(1 - V_k^{bc}\right)}. \tag{8}$$

2.5 Maximization of VSI (J_3)

The third objective function J_3 is utilized to maximize the voltage stability index of the system [35]. Mathematically, J_3 can be defined as:

$$J_3 = Minimize\left(\left(VSI\left(k\right)\right)^{-1}\right). \tag{9}$$

The VSI of the receiving end bus *k* of a branch *jk* can be expressed as provided by (10):

$$VSI(k) = \left\{V_j^2 - 2(P_k\ R_{jk} + Q_k\ X_{jk})\right\}^2 - 4(P_k^2 + Q_k^2)\ (R_{jk}{}^2 + X_{jk}{}^2)\,. \quad (10)$$

2.6 Minimization of the ICRI (J_4)

The optimal planning of DG and DSTATCOM units in the RDN might reduce the amount of capital expenditure needed to install such units. In addition to this, ICRI is employed for optimal sizing of DG and DSTATCOM units to achieve the most cost-effective deployment while adhering to technical constraints. A lower ICRI value indicates a more economical integration of DG and DSTATCOM into the RDN while maximizing technical advantages [5, 13, 36]. Mathematically, J_4 can be defined as:

$$J_4 = Minimize(ICRI)\,. \quad (11)$$

The ICRI can be computed based on the installation costs of DG and DSTATCOM and their costs at the maximum penetration limit at the optimal nodes [31], as given by (12). In addition to this, the total cost of DG and DSTATCOM is converted to annual costs using the economic life of the devices and the interest rate [5, 13, 36]:

$$ICRI = \frac{\left\{C_{dg}\sum_{i=1}^{N_{dg}} P_{dg,i}\,\frac{\alpha(1+\alpha/100)^{N_D}}{(1+\alpha/100)^{N_D}-1}\right\} + \left\{C_{dst}\sum_{i=1}^{N_{dst}} Q_{dst,i}\,\frac{\nu(1+\nu/100)^{N_S}}{(1+\nu/100)^{N_S}-1}\right\}}{C_{IC_{\max}}^{DG} + C_{IC_{\max}}^{DST}}, \quad (12)$$

where $C_{IC_{\max}}^{DG}$ and $C_{IC_{\max}}^{DST}$ are the total installation costs of DG and DSTATCOM units at their maximum rating in [$], respectively.

2.7 Constraints

The MOF is subjected to several system constraints that need to be satisfied [18]. These inequality and equality constraints are discussed in this section as follows:

Power balance equations: The limitations on the real and reactive power balances are specified by (13) and (14), respectively.

$$P_{ss} + \sum_{i=1}^{N_{dg}} P_{dg,i} = P_{load} + P_{cs} + P_{loss}\,, \quad (13)$$

$$Q_{ss} + \sum_{i=1}^{N_{dst}} Q_{dst,i} = Q_{load} + Q_{loss}\,. \quad (14)$$

Limits of bus voltage: The voltage at each bus should be maintained within a certain range to ensure that the system operates stably. The voltage constraint for each bus in the RDN is expressed by (15):

$$0.95 < V_k\,(p.u.) < 1.05\,. \quad (15)$$

VSI limitations: The VSI of each bus must be greater than zero to ensure the stable operation of the system, as specified by (16).

$$VSI\left(k\right) \geq 0 \quad for \quad k = 2,3,\ldots,N_{bus} \,. \tag{16}$$

DG and DSTATCOM rating limits: The capacity of individual DG and DSTATCOM units is limited by their maximum and minimum rating as specified by (17) and (18), respectively:

$$P_{dg,\min}^{k} < P_{dg}^{k} < P_{dg,\max}^{k} \,, \tag{17}$$

$$Q_{dst,\min}^{k} < Q_{dst}^{k} < Q_{dst,\max}^{k} \,. \tag{18}$$

The constraints for the total installed capacity of DG and DSTATCOM units are specified by (19) and (20), respectively:

$$\sum_{i=1}^{N_{dg}} P_{dg,i} < P_{load} \,, \tag{19}$$

$$\sum_{i=1}^{N_{dst}} Q_{dst,i} < Q_{load} \,. \tag{20}$$

Radiality constraint: The constraint that ensures the existence of radial topology in a network is provided by (21):

$$\left|BIM\right| = 1 \,. \tag{21}$$

3 Proposed Methodology

The details of the Cheetah Optimization Algorithm (COA) and its application are discussed in Subsections 3.1–3.2, subsequently.

3.1 Overview of COA

COA is a nature-inspired optimization approach proposed by [24]. COA is inspired by cheetah hunting techniques. Cheetahs hunt by seeking out their prey, waiting, and then launching an attack. The leave the prey and return home method is also used in the hunting process to increase population diversity, convergence performance, and the robustness of the suggested framework. The strategies [24] involved in COA are presented in Figs. 2a–2d. The flowchart of suggested algorithm is depicted in Fig. 3.

A) Search strategy

To obtain food, cheetahs have to look throughout their territories (search space) and in the surrounding area. The searching strategy of cheetahs may be mathematically modelled by using the notation $Z_{i,j}^{t}$ to express the current location of cheetah *i* in arrangement *j*. Different types of prey are encountered by each individual cheetah. The different states of cheetah constitute a population, and each individual prey is a decision variable that corresponds to the optimal

option. Thereafter, the new location of cheetah *i* in each arrangement are updated based on their previous position and an arbitrary step size, as given in (22):

$$Z_{i,j}^{t+1} = Z_{i,j}^{t} + \Upsilon_{i,j}^{-1}\mu_{i,j}^{t}, \quad i = 1, 2, \ldots, n, \; j = 1, 2, \ldots, d, \tag{22}$$

$$\mu_{i,j}^{t} = 0.0001(t / T_{ht})\left(U_b(j) - L_b(j)\right), \tag{23}$$

where $Z_{i,j}^{t+1}$, $Z_{i,j}^{t}$, $\Upsilon_{i,j}^{-1}$ and $\mu_{i,j}^{t}$ represent the next position, the current positions, randomization parameter and the step length of cheetah *i* in arrangement *j*, respectively. U_b and L_b are the upper and lower limits of search space. The position of the cheetah (leader) is updated in each cheetah arrangement by assuming the step length $\mu_{i,j}^{t}$ as provided by (23), while the locations of the remaining cheetahs are updated by assuming the step length $\mu_{i,j}^{t}$ as given by (24). Locating the neighboring member of the cheetah involves the following steps: i) Randomly choose a member of the cheetah population. ii) Iterate over the chosen members. iii) For each selected individual, check whether it is the last member of the population. iv) If it's the last member, choose the preceding member as the neighboring agent. v) Choose the next member as the neighbor agent if it's not the last.

$$\mu_{i,j}^{t} = 0.0001(t / T_{ht})\,\mathrm{abs}(X_{leader} - Z_{i,j}^{t}) + A_p, \tag{24}$$

where t is the current hunting time, and T_{ht} is the maximum length of hunting time. X_{leader} is the leader position, and A_p is random number which is equal to 0.001 times of the rounded value of a random number generated between 0 and 1 (i.e., 1 if the random number > 0.9, else 0).

B) Sit-and-wait strategy

Cheetahs come across their prey when they are actively looking for it. Every action that the cheetah does in this circumstance has the potential to notify the target animal, causing it to break up the pursuit and run away. To avoid this concern, the cheetah could try to ambush its prey by hiding behind some shrubs or lying down on the ground. Therefore, when operating in this mode, the cheetah waits for its prey to get closer to it (Fig. 2b). This behavior may be modelled as (25):

$$Z_{i,j}^{t+1} = Z_{i,j}^{t}, \tag{25}$$

where $Z_{i,j}^{t+1}$ and $Z_{i,j}^{t}$ are updated and current locations of cheetah *i* in arrangement *j*, respectively. This technique needs the COA to not alter all the cheetahs in each group at the same time in order to prevent premature convergence and improve hunting.

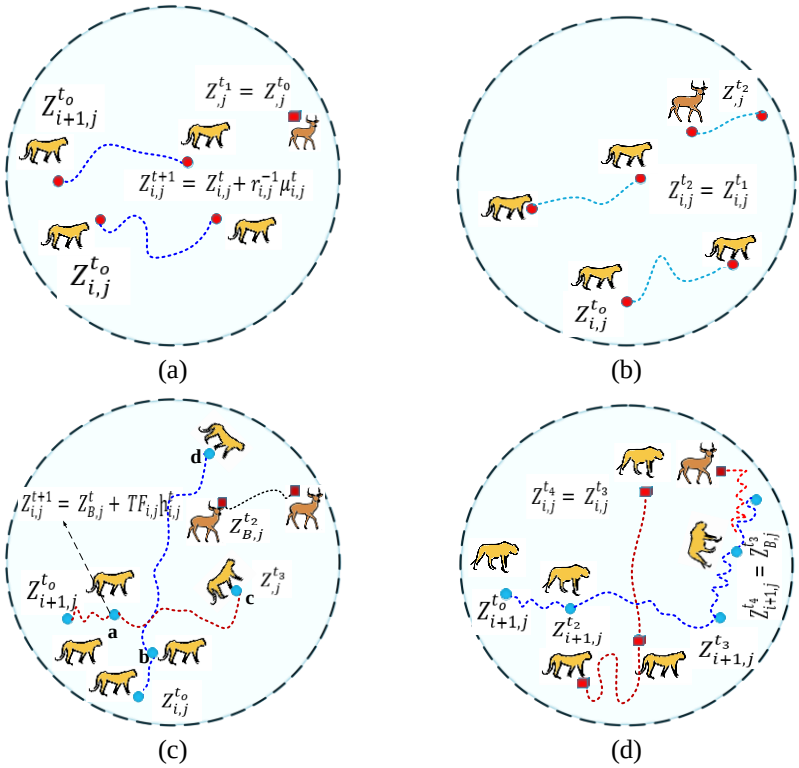

Fig. 2 – (a) *Searching strategy;* (b) *Sitting-and-waiting strategy;* (c) *Searching strategy;* (d) *Capturing strategy of Cheetah [24].*

C) Attack strategy

Cheetahs are able to successfully hunt because of their speed and their suppleness. Cheetahs are known to run up to their prey before making an attack. After a short period of time, the prey becomes aware of the cheetah's attack and runs away. The cheetah moves very swiftly in pursuit of the prey along the direction of the interception, as can be shown in Fig. 2c. To put it another way, the cheetah tracks its prey and modifies its motion such that it can outmaneuvers the prey at some time. Because the cheetah's next location is close to the prey's previous position, as illustrated in Fig. 2d, the prey needs to run away and change its position as rapidly as possible in order to live. During a collective hunt, it is possible for each cheetah to modify its location in response to the prey and the leader. These cheetah assault tactics are mathematically stated as (26) – (28):

$$Z_{i,j}^{t+1} = Z_{B,j}^{t} + TF_{i,j}\mathrm{H}_{i,j}^{t} \tag{26}$$

$$H_{i,j}^{t} = X_{i,j}^{nb} - Z_{i,j}^{t}, \tag{27}$$

$$TF_{i,j} = \text{abs}(rand)^{exp(rand/2)} \sin(2\pi rand)\,, \tag{28}$$

where $Z_{B,j}^{t}$ is the location of the prey in arrangement *j*; $X_{i,j}^{nb}$ is the neighbor position; $TF_{i,j}$ and $\mathrm{H}_{i,j}^{t}$ are Cheetah *i*'s turning factor and interaction factor in arrangement *j*, respectively. Cheetahs, while in an attacking mode, utilize their maximal speed to swiftly narrow the distance between themselves and their prey; hence, $Z_{B,j}^{t}$ is employed in (26).

D) Hypotheses

In hunting, the searching or attacking approach is employed randomly, although the searching method becomes more probable with time owing to depleting cheetah energy. In other circumstances, the search strategy comes first, whereas the attack method is used for high values of t to produce better results. If $rand_2 > rand_3$, the sit-and-wait approach is chosen; otherwise, one of the seeking or assaulting strategies is chosen based on a random value R, as given by (29) and (30):

$$Z_{i,j}^{t+1} = \begin{cases} \text{Eq. (26)}, & \text{if } rand_2 \le rand_3 \ \&\ R \ge rand_4, \\ \text{Eq. (22)}, & \text{if } rand_2 \le rand_3 \ \&\ R \le rand_4, \\ \text{Eq. (25)}, & \text{if } rand_2 > rand_3, \end{cases} \tag{29}$$

$$R = \mathrm{e}^{2(1-t/T_{It})}\,(2rand_1 - 1)\,, \tag{30}$$

where $rand_1$, $rand_2$ and $rand_3$ are random number from the range [0, 1]. $rand_4$ is a random number from 0 to 3. Tuning rand_3 controls the switching rate between sit-and-wait and two additional strategies. Higher $rand_4$ values prioritize the exploitation phase, whereas lower values prioritize the exploration phase.

3.2 Application of COA

In this work, COA is employed to solve the problem of simultaneous optimal placement of EVCS with NR and planning of DG and DSTATCOM units on the RDN. During the optimization process, the Cheetah positions are considered as potential solution for the problem of optimal placement of EVCSs with NR and planning of DG and DSTATCOM units on the RDN. The algorithm searches for the optimal combination of these variables that minimizes the MOF, while satisfying the system constraints. The following are the suggested steps for solving the optimal allocation problem of EVCS with compensating devices and NR using COA.

1. Enter the bus data, branch data, and EVCS load data, as well as algorithm parameters (*d*, *n* and maximum iterations ($It_{\max}$)).
2. Generates an initial population of cheetahs randomly in the search space using (31), as given by (32).

$$Zp_i = L_b + [rand(1,d) \times (U_b - L_b)], \tag{31}$$

$$Zp = \begin{bmatrix} z_{1,1}, z_{1,2}, z_{1,3}, \ldots z_{1,d} \\ z_{2,1}, z_{2,2}, z_{2,3}, \ldots z_{2,d} \\ \vdots \\ z_{n,1}, z_{n,2}, z_{n,3}, \ldots z_{n,d} \end{bmatrix}, \tag{32}$$

where Zp_i represented a cheetah or a solution vector of dimensions *d*; Zp represents the initial population of cheetahs in the search space as a matrix of size $(n \times d)$; *rand* is a random number generator. Each column of the matrix Zp represents a decision variable of the optimization problem. Furthermore, each row of the matrix Zp represents a possible solution (i.e., a cheetah), as given in (33):

$$\begin{aligned} Zp_i = [&\underbrace{TS_1, TS_2, \ldots, TS_{Tsw}}_{\text{Switches status}}, \underbrace{EV_1, EV_2, \ldots, EV_{Kev}}_{\text{EVCS location}}, \underbrace{D_1, D_2, ..., D_{N_{dg}}}_{\text{DG location}}, \\ &\underbrace{DS_1, DS_2, \ldots, DS_{N_{dg}}}_{\text{DG size}}, \underbrace{C_1, C_2, \ldots, C_{N_{dst}}}_{\text{DSTATCOM location}}, \underbrace{CS_1, CS_2, \ldots, CS_{N_{dst}}}_{\text{DSTATCOM size}}], \end{aligned} \tag{33}$$

where the subscript *Kev* and T*sw* denote total number of EVCS and opened switches for optimal NR, respectively; $(D_1, D_2, \ldots, D_{N_{dg}})$ are the locations of DG units, and the corresponding DG sizes are denoted by $(DS_1, DS_2, \ldots, DS_{N_{dg}})$. The locations of DSTATCOM units are denoted by $(C_1, C_2, \ldots, C_{N_{dst}})$, and the corresponding DSTATCOM sizes are denoted by $(CS_1, CS_2, \ldots, CS_{N_{dst}})$. The locations for multiple EVCS installation are denoted by $(EV_1, EV_2, \ldots, EV_{Kev})$, and the open switches for optimal NR are denoted by $(TS_1, TS_2, \ldots, TS_{Tsw})$.

3. For each randomly produced solution, compute the fitness value.
4. Verify the system's constraints for each initial population solution.
5. Select the best solution from the initial population as the initial leader position. Also, initialize the current position of i^{th} cheetah, neighbour position, and the prey position. The home position represents the best solution found so far, the leader position represents the best solution among the neighbouring solutions, and the prey position represents the global best solution.
6. Initialize the iteration, hunting time counters, and the function evaluation counter.
7. Start the main loop: The algorithm starts the main loop that will continue until the maximum iterations achieved ($FEC \leq It_{\max}$).

8. Select a random set of m cheetahs from the population and algorithm iterates over the selected cheetahs and applies the different strategy to each one of them.
9. For each cheetah in the selected set, the algorithm selects a neighbour cheetah.
10. The COA utilizes three different strategies for the cheetahs to search for prey and improve their solutions, as given by (34):

$$Strategy = \begin{cases} Attack\ Strategy & \text{if } rand_2 \le rand_3 \ \&\ R \ge rand_4, \\ Search\ Strategy & \text{if } rand_2 \le rand_3 \ \&\ R < rand_4, \\ Sit\ \&\ Wait\ Strategy & \text{if } rand_2 > rand_3. \end{cases} \quad (34)$$

Search Strategy: When cheetah does not detect any prey nearby (i.e., $rand_2 \le rand_3 \ \&\ R \ge rand_4$) it uses this strategy to move to a new location in the search space. The new position is calculated using (22) where a random number $\Upsilon_{i,j}^{-1}\mu_{i,j}^{t}$ is added to the current position of i^{th} cheetah to introduce some randomness into the movement as given by (35):

$$\begin{aligned} Z_{i,j}^{t+1} = [&TS_1^c,\ldots,TS_{Tsw}^c,\ EV_1^c,\ldots,EV_{Kev}^c,\ D_1^c,\ldots,D_{N_{dg}}^c, \\ &DS_1^c,\ldots,DS_{N_{dg}}^c,\ C_1^c,\ldots,C_{N_{dst}}^c,\ CS_1^c,\ldots,CS_{N_{dst}}^c] + \Upsilon_{i,j}^{-1}\mu_{i,j}^{t}, \end{aligned} \quad (35)$$

where superscript *c* is used to denote the current position of i^{th} cheetah.

Attack Strategy: When a cheetah detects prey nearby (*i.e.*, $rand_2 \le rand_3 \ \&\ R < rand_4$), it uses this strategy to move towards the prey's location and attempt to catch it. The new position is calculated using (26) where $TF_{i,j}\mathrm{H}_{i,j}^{t}$ is added to the prey position to introduce some randomness into the attack as given by (36):

$$\begin{aligned} Z_{i,j}^{t+1} = [&TS_1^P,\ldots,TS_{Tsw}^P,\ EV_1^P,\ldots,EV_{Kev}^P,\ D_1^P,\ldots,D_{N_{dg}}^P, \\ &DS_1^P,\ldots,DS_{N_{dg}}^P,\ C_1^P,\ldots,C_{N_{dst}}^P,\ CS_1^P,\ldots,CS_{N_{dst}}^P] + TF_{i,j}\mathrm{H}_{i,j}^{t}, \end{aligned} \quad (36)$$

where superscript *P* is used to denote the prey position in arrangement *j*.

Sit-and-wait strategy: When a cheetah detects prey nearby but is not close enough to attack (*i.e.*, $rand_2 > rand_3$), it uses this strategy to stay in its current position and wait for the prey to come closer as given by (37).

$$\begin{aligned} Z_{i,j}^{t+1} = [&TS_1^c,\ldots,TS_{Tsw}^c,\ EV_1^c,\ldots,EV_{Kev}^c,\ D_1^c,\ldots,D_{N_{dg}}^c, \\ &DS_1^c,..DS_{N_{dg}}^c,\ C_1^c,\ldots,C_{N_{dst}}^c,\ CS_1^c,\ldots,CS_{N_{dst}}^c], \end{aligned} \quad (37)$$

11. Updates the Function Evaluation Counter (FEC) and the best cheetah in the population.
12. Update hunting time counters (t).

13. If $t > T_{ht} rand$ and the leader position does not change for a period of time, then implement the leave the prey and return home strategy and modify the leader position (i.e., replace the position of member *i* with the prey position).
14. Iterate through steps 7–13 until the maximum allowed number of iterations is achieved.
15. Return the best cheetah's position (i.e., optimal solution).

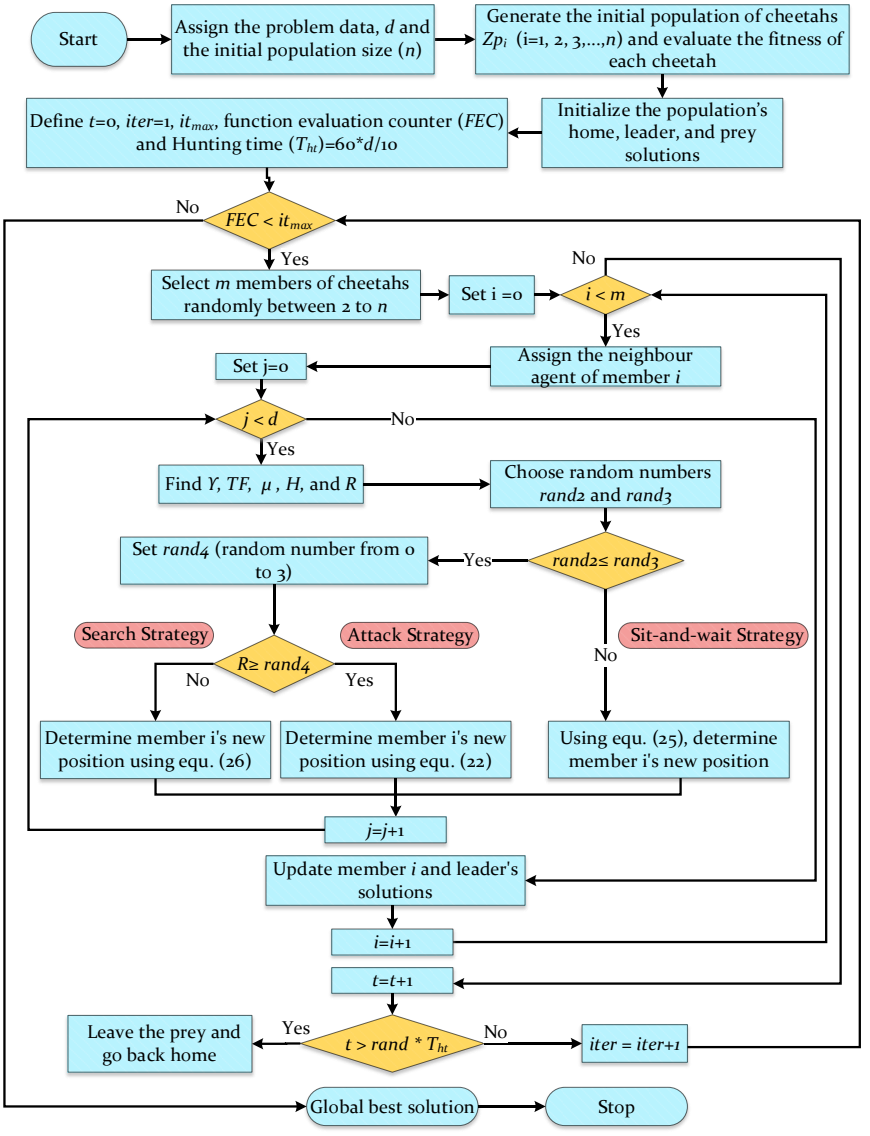

Fig. 3 – COA flowchart.

4 Results and Discussions

This research considers renewable energy type DG, which generates power at unity power factor, while DSTATCOM delivers reactive power. EVCS are presumed to have 25 charging outlets, and each charger's power demand is 40 kW. Therefore, 25 EVs can be charged at the same time via charging stations. The maximum power consumption of an EVCS is 1 MW when all of its charging points are utilized for charging EVs at the same time. The best location in the distribution network must be chosen for the placement of charging stations. Due to the placement of EVCS, the network's real power loss rises, and the voltage profile of the buses is disrupted. As a result, DGs or DSTATCOMs must be well-positioned to mitigate the impacts of EVCS on the RDN.

In this study, the power flow analysis on the RDN is done using the forward/backward sweep approach in this work [37]. Simulations are run on an Intel i7 computer with 3.0GHz and 8GB of RAM using MATLAB. The suggested COA is applied to two distribution systems. These systems are the 33-bus [38] and the 136-bus RDN [25]. The parameters for ICRI calculation are taken from [4, 5, 39], as shown in **Table 2**. To achieve a balance between technical and economic advantages, proper consideration of weighting factors is essential. In this study, an analytical test on a 136-bus RDN with EVCS and DG units is conducted to determine the most effective values of weighting factors, enabling the assessment of the optimal value of MOF with a balanced technical and economic advantage. The impact of different combinations of weighting factor values on MOF components are shown in **Table 3**.

Table 2
Economic data for DG and DSTATCOM allocation.

Parameters	C_{dg}	C_{dst}	α	ν	N_D	N_S
Values	500 $/kW	50$/KVAr	10	10	20	30

4.1 Different case studies

Four operational cases are presented to evaluate the effectiveness of the COA and study the impact of EVCSs in combination with DGs, DSTATCOMs, and optimal NR on the system performance.

Base case: RDN without EVCS, DG, and DSTATCOM.

Case 1: Integration of EVCSs into RDN (with and without NR).

Case 2: Simultaneous integration of EVCSs and DSTATCOMs into RDN (with and without NR).

Case 3: Simultaneous integration of EVCSs and DGs into RDN (with and without NR).

Case 4: Simultaneous integration of EVCSs, DGs, and DSTATCOMs into RDN (with and without NR).

Table 3
Weighting factor values and various indices.

Weighting factors				IRPL	VSI	RPL [kW]	ITVD	EVCS location	DG size [MW] and location	Total DG capacity [MW]	DG cost [$]
β_1	β_2	β_3	β_4								
0.7	0.1	0.1	0.1	0.3466	0.8560	111.03	0.6184	14, 106, 84, 90, 28, 52	1.699 (86), 2.77 (44), 1.437 (101), 1.642 (100), 1.8 (64), 2.805 (76)	12.152	713709.1
0.6	0.2	0.1	0.1	0.3712	0.8643	118.92	0.6583	90, 9, 82, 106, 131, 49	1.718 (122), 2.85 (64), 1.175 (7), 2.9 (3), 1.393 (100), 1.863 (86)	11.899	698833.5
0.5	**0.2**	**0.2**	**0.1**	**0.3658**	**0.8714**	**117.19**	**0.6178**	107, 91, 53, 84, 32, 9	2.798 (100), 1.377 (64), 1.764 (122), 1.463 (18), 2.062 (76), 2.176 (77)	**11.640**	**683650.1**
0.5	0.3	0.1	0.1	0.3869	0.8608	123.96	0.6553	7, 53, 85, 108, 32, 90	2.372 (40), 2.727 (18), 0.787 (54), 2.316 (76), 1.986 (2), 1.893 (100)	12.080	709433.7
0.4	0.3	0.2	0.1	0.4502	0.8871	144.23	0.6495	84, 106, 109, 57, 9, 93	2.306 (100), 1.924 (40), 1.046 (43), 2.101 (84), 3 (3), 1.681 (86)	12.058	708173.9
0.3	0.3	0.3	0.1	0.4562	0.8891	146.14	0.6175	106, 49, 109, 93, 29, 14	1.997 (2), 2.816 (41), 1.122 (19), 1.823 (64), 2.752 (40), 1.528 (18)	12.037	706932
0.6	0.1	0.1	0.2	0.4295	0.8719	137.59	0.6645	111, 32, 84, 16, 106, 48	0.899 (18), 2.171 (2), 2.093 (84), 1.844 (106), 3 (100), 1.83 (19)	11.836	695146.1
0.5	0.2	0.1	0.2	0.4611	0.8763	147.73	0.6841	81, 14, 35, 132, 107, 49	1.492 (76), 0.894 (64), 1.598 (50), 3 (122), 3 (40), 0.2 (101)	10.184	598088.9
0.4	0.2	0.2	0.2	0.4921	0.8887	157.64	0.6925	7, 117, 53, 106, 131, 14	0.218 (122), 0.586 (53), 3 (131), 2.47 (86), 2.343 (2), 2.052 (40)	10.669	626561.5
0.3	0.3	0.2	0.2	0.4714	0.8894	151.00	0.6281	36, 54, 84, 108, 35, 95	1.501 (18), 3 (54), 1.232 (100), 2.953 (122), 0.589 (64), 1.2 (86)	10.475	615195.6
0.4	0.2	0.1	0.3	0.4809	0.8616	154.07	0.7157	95, 28, 53, 84, 106, 134	0.959 (40), 1.257 (18), 2.059 (122), 0.581 (41), 2.822 (76), 0.838 (64)	8.517	500197.5
0.3	0.2	0.2	0.3	0.5335	0.8831	170.93	0.7066	7, 108, 37, 49, 10, 37	1.486 (37), 2.89 (100), 0.351 (101), 1.985 (40), 0.2 (64), 1.737 (2)	8.649	507930.8

According to **Table 3**, the DG penetration decreases as the β_4 value increases. Consequently, the technical advantage diminishes. Also, there is close competition between the first six combinations of the weighting factors. Furthermore, the values of β_1, β_2, β_3 and β_4 at 0.7, 0.1, 0.1, and 0.1 have the lowest MOF but have a lesser impact on ITVD and VSI. The values of β_1, β_2, β_3 and β_4 at 0.5, 0.2, 0.2, and 0.1 have a stronger impact on ITVD, IRPL, VSI, and the DG investment cost. As a result, the values of β_1, β_2, β_3 and β_4 considered are 0.5, 0.2, 0.2, and 0.1, respectively.

The case studies for 33 and 136 bus networks are discussed in Subsection 5.2-5.3, subsequently.

4.2 For 33-bus RDN

The one-line diagram of the 33-bus RDN is depicted in Fig. 4 [30, 38]. The system has a total real power load requirement of 3.715 MW and a reactive power load requirement of 2.3 MVAr. The network consists of 33 buses, 37 branches, 32 selection switches, 5 tie switches, and 5 fundamental loops. The system operates at a rated line voltage of 12.66 kV with a base MVA rating of 10. Furthermore, three EVCS are considered for integration into the 33-bus RDN to meet customer demand and ensure EVCS availability for a significant number of EV customers. The different operational cases of the 33-bus RDN are as follows:

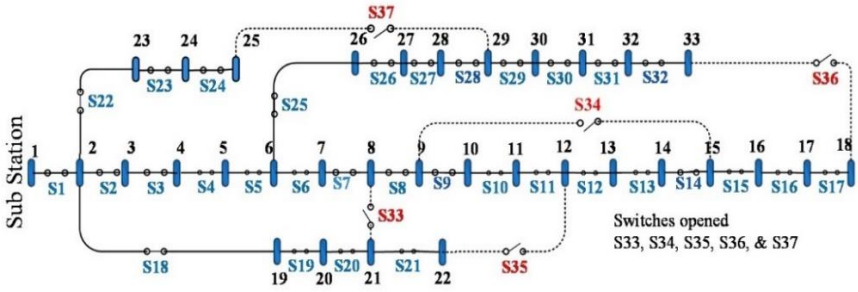

Fig. 4 – *Standard 33-bus RDN.*

4.2.1 Case 1

In this case, EVCSs are integrated into the system without considering DGs and DSTATCOMs to evaluate the impact of charging station load on the RDN. Furthermore, technical aspects such as IRPL, ITVD, and Minimum VSI (MVSI) are taken into consideration for MOF. Additionally, the impacts of EVCS installation on RDN are analyzed using two scenarios, WONR and WNR.

A) Scenario 1 (WONR)

In this scenario, the MOF is optimized by determining the optimal bus positions for EVCS installations using the COA. **Table 4** presents the simulation results for this scenario. The potential bus locations considered for EVCS

installations are 2, 19, and 20, as provided in **Table 5**. The resulting IRPL, ITVD and MVSI values are 1.1933, 1.05387 and 0.6614, respectively. Furthermore, the value of RPL and minimum bus voltage are 251.78 kW and 0.9018 p.u., respectively. In addition to this, the VS tolerance limit for each bus voltage is not kept within the permissible range of ±5%.

Table 4

Performance analysis of the 33-bus RDN with four cases.

Cases	Scenario	IRPL	MVSI	ITVD	Vmin (p. u.) & bus number	Total size of DG [MW]/ DSTATCOM [MVAr]	RPL [kW]
Base case	---	---	---	---	0.9037 & 18	---	211
Case 1	WONR	1.1933	0.6614	1.05387	0.9018 & 18	---	251.78
	WNR	0.8638	0.7679	0.66483	0.9361 & 32	---	182.27
Case 2	WONR	0.8799	0.7388	0.80340	0.9271 & 18	---/1.12	185.66
	WNR	0.6582	0.8377	0.55472	0.9567 &32	---/1.15	138.87
Case 3	WONR	0.4696	0.9087	0.25053	0.9764 &33	3.180/---	99.07
	WNR	0.3496	0.9145	0.24959	0.9779 & 33	3.357/---	73.77
Case 4	WONR	0.2370	0.9065	0.22467	0.9757 &18	3.034/1.079	50.01
	WNR	0.1754	0.9446	0.14244	0.9859 & 24	3.160/1.065	37.00

B) Scenario 2 (WNR)

In this scenario, the potential bus locations for the EVCS installation are determined in coordination with the optimal network reconfiguration by optimizing the MOF via the COA. In comparison to the WONR scenario, when the RDN is reconfigured with three EVCSs, RPL decreases to 182.27 kW from 251.78 kW, VSI increases to 0.7679 from 0.6614, and the minimum bus voltage increases to 0.9361 from 0.9018 p. u., as shown in **Table 4**. Moreover, scenario 2 further lowers the IRPL value by 27.61 percent in comparison to WONR scenario. From Fig. 5, it is seen that the VPs of each node do not follow the VS limit of ± 5%.

4.2.2 Case 2

The integration of EVCSs has an additive influence on RPL and a negative impact on the VP and VSI, as shown in case 1. The inclusion of DSTATCOM units at the optimal nodes can compensate for these disruptions. In this case, the MOF considers both technical factors (IRPL, ITVD, and VSI) and economic factors (the cost of investing in DSTATCOM installation). Furthermore, the EVCS are optimally allocated in coordination with DSTATCOM by optimizing the MOF using COA under two distinct scenarios.

A) Scenario 1 (WONR)

In this scenario, the impact of EVCS' integration in coordination with DSTATCOM units on IRPL, ITVD, VSI and ICRI is studied for the 33-bus RDN, and results are provided in **Table 4**. Three DSTATCOMs are installed at buses 31, 30, and 14, with penetrations of 0.3127, 0.4732, and 0.3641 MVAr, respectively. The potential bus locations for EVCS installation are 2, 20, and 19. Due to reactive power compensation by DSTATCOM, it can be noticed that RPL and ITVD are significantly decreased as compared to case 1, whereas VSI is significantly improved. In addition to this, the resultant values of IRPL, ITVD, and MVSI are 0.8799, 0.8034, and 0.7388, respectively. The value of RPL and minimum bus voltage are 185.66 kW and 0.9271 p. u., respectively. As shown in Fig. 5, the system's voltage profile improves when EVCS and DSTATCOM are simultaneously placed on RDN. From **Table 4**, it is seen that installing EVCS, with or without NR, does not achieve the desired results of minimizing IRPL, ITVD, and VSI reduction.

B) Scenario 2 (WNR)

In this scenario, the impact of EVCS' integration in coordination with DSTATCOM units and NR on various performance indices is studied for the 33-bus RDN, and results are provided in **Table 4**. The switches S7, S9, S14, S37, and S32 are opened during NR. The candidate bus locations for EVCS are 2, 3, and 19. The potential bus locations for DSTATCOM installation are 30, 32, and 17, with penetrations of 0.6431, 0.2591, and 0.2478 MVAr, respectively. Compared to scenario 1 of case 2, the suggested COA technique reduces RPL to 138.87 kW from 185.66 kW, a reduction of 25.2%. In addition to this, the MVSI value is improved from 0.7388 to 0.8377, and the minimum bus voltage is increased from 0.9271 to 0.9567 p. u. From **Table 4**, it is seen that improvements in IRPL reduction, ITVD reduction, and MVSI maximization are higher when compared to scenario 1 of case 2.

4.2.3 Case 3

As observed in case 2, the inclusion of EVCS in coordination with DSTATCOM units at the optimal nodes does not yield the desired results of maximizing IRPL reduction, ITVD reduction, VSI improvement and ICRI reduction. As a result, the EVCS are optimally allocated in coordination with DG units by optimizing the MOF via COA under two distinct scenarios, WONR and WNR. In this case, the MOF considers both technical factors (IRPL, ITVD, and VSI) and economic factors (cost of investing in DG).

A) Scenario 1 (WONR)

In this scenario, the impact of EVCS' integration in coordination with DG units on IRPL, ITVD, VSI and ICRI is studied for the 33-bus RDN, and results are provided in **Table 4**. Three DG units are installed at optimal buses 25, 30, and 13, with penetrations of 0.66, 1.35, and 1.17 MW, respectively. The potential bus locations for EVCS installation are 2, 3, and 19. As a result of active power compensation by DGs units, it is seen that IRPL, ITVD, and VSI reduction have all minimized significantly compared to cases 1 and 2 of the 33-bus RDN. The values of RPL and minimum bus voltage are 99.07 kW and 0.9764 p. u., respectively. In comparison to cases 1 and 2, integrating EVCS with DGs units significantly improved the VP of the 33-bus network, as shown in Fig. 5. Furthermore, the power loss in each branch is also reduced by integrating EVCS with DGs.

Table 5

Optimal site and size of compensating devices for allocation on 33-bus RDN.

Cases	Scenario	EVCSs locations	DG sizes [MW] and sites	DSTATCOM sizes [MVAr] and sites	Switches opened
Case 1	WONR	2, 19, 20	---	---	S33-S37
	WNR	2, 3, 19	---	---	S9, S7, S14, S32, S28
Case 2	WONR	2, 20, 19	---	0.3127 (31), 0.4732 (30), 0.3641(14)	S33-S37
	WNR	2, 3, 19	---	0.6431 (30), 0.2591 (32), 0.2478 (17)	S7, S9, S14, S37, S32
Case 3	WONR	3, 2, 19	0.66 (25), 1.35 (30), 1.17 (13)	---	S33-S37
	WNR	3, 19, 2	0.72 (14), 0.75 (8), 1.887 (29)	---	S11, S6, S34, S32, S28
Case 4	WONR	19, 2, 32	0.777 (9), 0.580 (10), 1.677 (31)	0.2531 (30), 0.6984 (31), 0.1275 (8)	S33-S37
	WNR	3, 19, 2	1.03 (21), 0.72 (18), 1.41 (29)	0.290 (25), 0.265 (18), 0.510 (30)	S11, S7, S34, S31, S24

B) Scenario 2 (WNR)

In this scenario, three EVCS are optimally located with the simultaneous incorporation of NR and three DG units. **Table 4** demonstrates the simulation result for this scenario. Fig. 6 represents a reconfigured 33-bus RDN with optimally positioned EVCS and DG units. The candidate bus locations for EVCS installation are 2, 3, and 19, as provided in **Table 5**. Three DG units are located

at buses 14, 8, and 29, with penetrations of 0.72, 0.75, and 1.887 MW, respectively. The switches S11, S6, S34, S32, and S28 are opened during NR. Compared to scenario 1 of case 3, the suggested COA technique reduces RPL to 73.77 kW from 99.07 kW, a reduction of 25.53%. In addition to this, the MVSI value is improved to 0.9145 from 0.9087 and the minimum bus voltage is increased from 0.9764 to 0.9779 p. u. In comparison to scenario 1 of case 3, scenario 2 significantly improved the VP of the 33-bus RDN. From Figs. 7–10, it is seen that improvements in IRPL reduction, ITVD reduction, and MVSI maximization are higher compared to cases 1 and 2 due to active power compensation by three DGs and optimal NR. According to Fig. 11, scenario 2 also minimizes power loss at each of the branches of the 33-bus RDN.

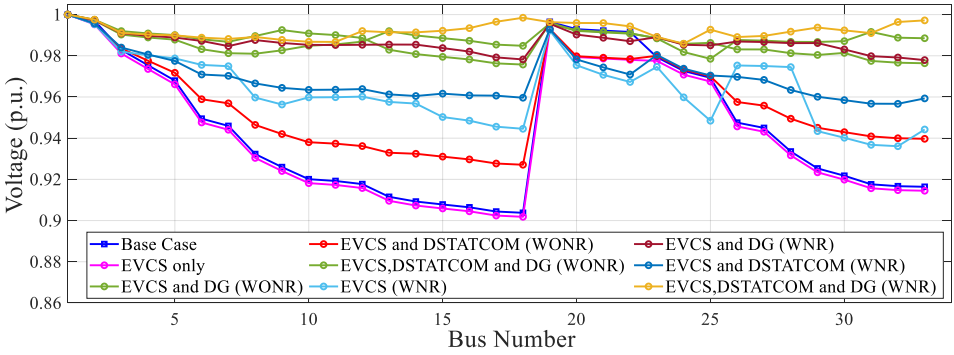

Fig. 5 – *VP for 33-bus RDN.*

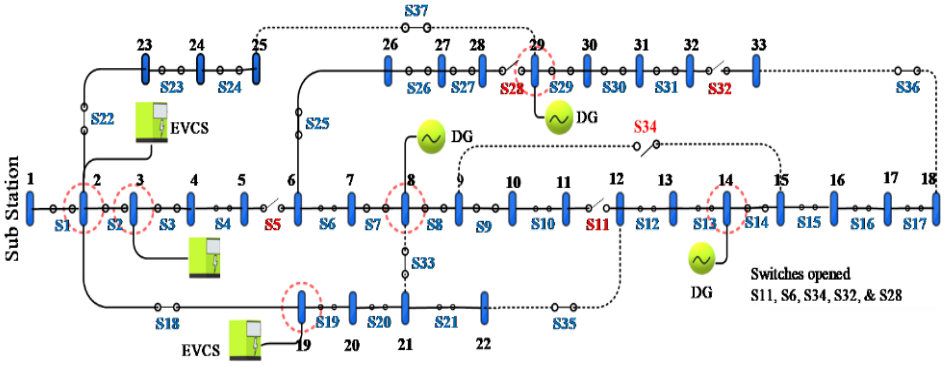

Fig. 6 – *Reconfigured 33-bus RDN with multiple EVCSs and DGs units.*

4.2.4 Case 4

To assess the impact of EVCSs installation with simultaneous integration of DG and DSTATCOM units on RDN, the MOF is optimized using COA under multiple scenarios. The following are the two possible scenarios:

A) Scenario 1 (WONR)

In this scenario, the potential bus locations for the EVCS installation are determined in coordination with the optimal site and size of the DGs and DSTATCOMs units by optimizing the MOF using COA. The results of the 33-bus RDN for this scenario are shown in **Table 4**. In this scenario, the actual and reactive power compensation by DGs and DSTATCOMs units considerably increases the IRPL reduction, ITVD reduction, and VSI maximization when compared to cases 1, 2, and 3. The resultant values of IRPL, ITVD, and MVSI are 0.2370, 0.22467, and 0.9065, respectively. Also, the minimum bus voltage is 0.9757 p.u., which is found on bus 18. The improved VPs of each bus for this scenario is shown in Fig. 5. In addition, simultaneous integration of EVCS, DGs, and DSTATCOMs lowers power loss in each branch of the network, as shown in Fig. 11.

B) Scenario 2 (WNR)

In this scenario, the potential bus locations for the EVCS installation are determined in coordination with the optimal NR as well as the optimal location and size of the DGs and DSTATCOMs units by optimizing the MOF via COA. **Table 4** shows the results of the 33-bus network based on scenario 2 of case 4. During NR, the switches S11, S7, S34, S31, and S24 are opened. Also, **Table 4** shows that case 4's scenario 2 is much superior to case 4's scenario 1 for the 33-bus network in terms of minimizing the IRPL, ITVD, and VSI reduction. Compared to scenario 1 of case 4, scenario 2 has a further 26.01 % drop in IRPL. Meanwhile, the minimum bus voltage rises from 0.9757 p.u. to 0.9859 p. u. and the VSI increases from 0.9065 to 0.9446. The improvement in IRPL reduction, ITVD reduction, and MVSI is highest for scenario 2 of case 4 compared to other cases of the 33-bus RDN, as shown in Figs. 7 – 9. Also, the power loss in each branch is significantly reduced, as shown in Fig. 11.

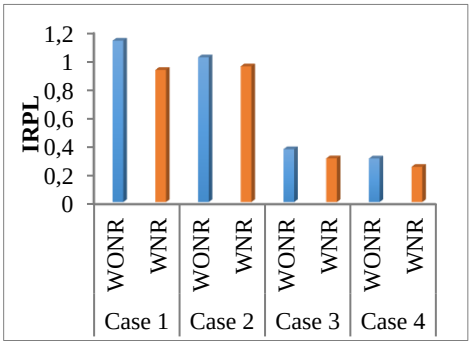

Fig. 7 – IRPL *for 33-bus RDN.*

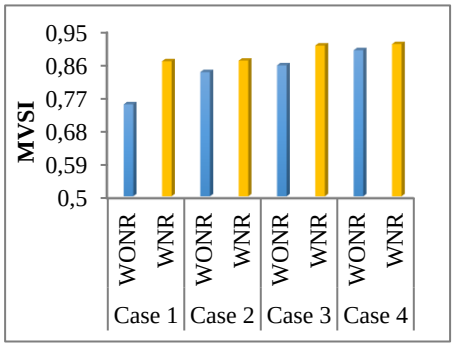

Fig. 8 – *MVSI for 33-bus RDN.*

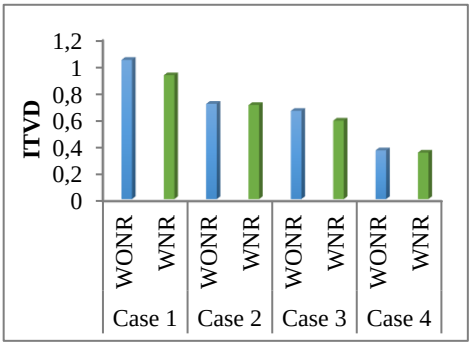

Fig. 9 – *ITVD for 33-bus RDN.*

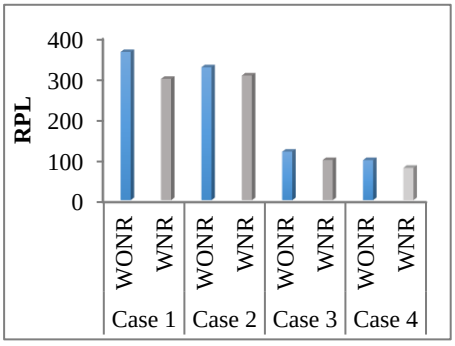

Fig. 10 – *RPL for 33-bus RDN.*

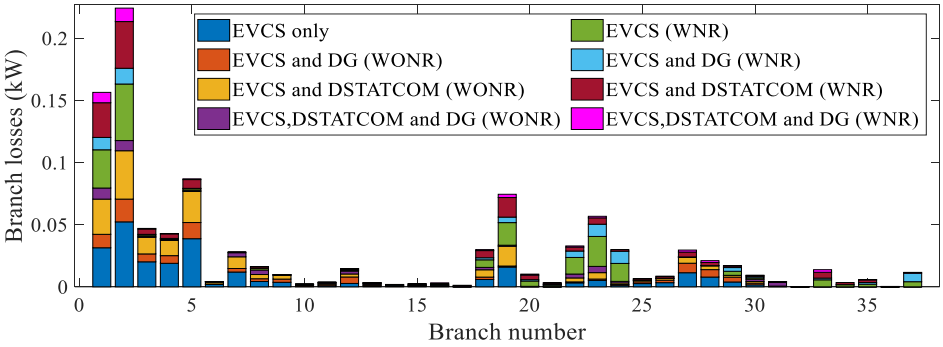

Fig. 11 – *Branch losses of 33-bus RDN* (*Case 1-4*).

4.3 For 136-bus network

The one-line diagram of 136-bus RDN is shown in Fig. 12 [30, 25]. In addition, the system's total real and reactive power load requirements are 18.31 MW and 7.93 MVAr, respectively. The network consists of 136 buses, 156 branches, 135 selection switches, 21 tie switches and 21 fundamental loops. The rated line voltage of the system is 13.88 kV, and its base MVA rating is 10. To fulfil customer demand and assure EVCS availability for a significant number of EV customers, six EVCS have been considered for installation on the 136-bus RDN. The different operational cases are as follows:

4.3.1 Case 1

In this case, EVCSs are integrated into the system without considering DGs and DSTATCOMs to evaluate the impact of charging station load on RDN. Furthermore, technical aspects such as IRPL, ITVD, and VSI are taken into consideration for MOF. Additionally, the impacts of EVCS installation on RDN are analyzed using two scenarios, WONR and WNR.

A) Scenario 1 (WONR)

In the same manner as the 33-bus RDN, the impact of EVCS' integration on IRPL, ITVD, and VSI is studied for the 136-bus RDN, and results are presented in **Table 6**. The candidate bus locations for EVCS installations in the 136-bus RDN are 76, 64, 2, 100, 67, and 40. Also, **Table 6** shows that the resultant IRPL, ITVD, and MVSI values are 1.1342, 1.0388, and 0.7499, respectively. The value of RPL and minimum bus voltage are 363.35 kW and 0.9306 p. u. Fig. 13 shows the voltage profiles of each node do not follow the VS tolerance limit of ± 5%.

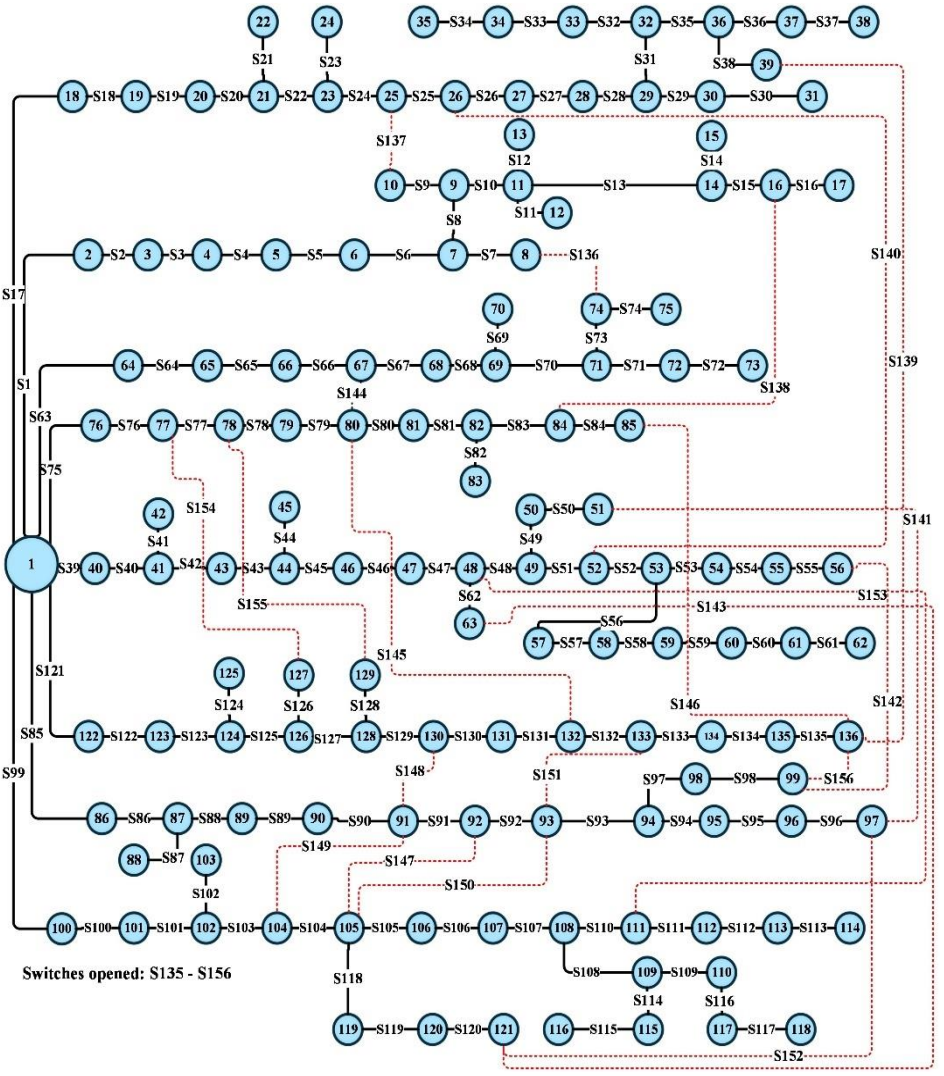

Fig. 12– *Standard 136-bus RDN.*

B) Scenario 2 (WNR)

In this scenario, the impacts of EVCS installation with optimal NR on IRPL, ITVD, and VSI are studied for the 136-bus RDN, and the results are presented in **Table 6**. The resulting IRPL, ITVD, and MVSI values are 0.9287, 0.9240, and 0.8672, respectively. The percentage reductions in IRPL and ITVD relative to the WONR scenario are 18.12 percent and 11.04 percent, respectively. The minimum voltage of 0.9650 p.u. is achieved at bus 61. From Fig. 13, it is seen that the VPs of each node follow the permissible range of VS limits of ± 5%.

Table 6
Performances analysis of the 136-bus RDN with cases 1 and 2.

	Case 1		Case 2	
Scenario	WONR	WNR	WONR	WNR
Vmin (p. u.)/bus	0.9306/117	0.9650/61	0.9566/117	0.9655/106
IRPL	1.1342	0.9287	1.0168	0.9538
MVSI	0.7499	0.8672	0.8375	0.8689
ITVD	1.0388	0.924	0.7109	0.7017
Total size [MVAr] of DSTATCOM	---	---	---/3.918	---/3.913
RPL [kW]	363.35	297.51	325.74	305.58
EVs locations	76, 64, 2, 100, 67, 40	86, 64, 100, 122, 76, 40	40, 86, 100, 64, 122, 4	43, 3, 18, 65, 64, 122
DSTATCOM sizes [MVAr]/ sites	---	---	1.3403 (49), 0.4732 (28), 0.7556 (113), 0.5006 (52), 0.1724 (108), 0.6760 (94)	1.0216 (109), 0.7153 (34), 0.5279 (82), 1.0124 (9), 0.100 (78), 0.5355 (134),
Switches opened	S136-S156	S136, S137, S138, S38, S51, S141, S54, S143-S152, S106, S126, S155, S156	S136-S156	S136, S9, S138, S38, S140, S141, S54, S143, S144-S152, S106, S126, S128, S156

4.3.2 Case 2

Similar to case 2 of the 33-bus network, the EVCS are optimally allocated in coordination with DSTATCOM by optimizing the MOF using COA under two distinct scenarios.

A) Scenario 1 (WONR)

The impacts of EVCS' integration in coordination with DSTATCOM units on various performance indices are studied for the 136-bus RDN. Six DSTATCOMs are installed at buses 49, 28, 113, 52, 108, and 94, with penetrations of 1.3403, 0.4732, 0.7556, 0.5006, 0.1724, and 0.6760 MVAr, respectively, as presented in **Table 6**. The candidate bus locations for EVCS

installation are 40, 86, 100, 64, 122, and 4. From **Table 6**, it is observed that the simultaneous integration of EVCS and DSTATCOM has an incremental impact on VSI while having a decremental impact on the IRPL and ITVD of the 136-bus RDN. The resultant IRPL, ITVD, and MVSI values are 1.0168, 0.7109, and 0.8375, respectively. The minimum bus voltage of 0.9566 p. u. is obtained at bus 117. Also, **Table 6** shows that improvements in RPL reduction, ITVD reduction, and MVSI are higher when compared to case 1 of the 136-bus network. Figs. 13 and 14 show that the VPs of each bus is improved and the power loss in each branch is reduced in scenario 1 of case 2.

B) Scenario 2 (WNR)

The integration of EVCSs with DSTATCOMs and optimal NR resulted in a reduction in ITVD and IRPL while increasing VSI of the 136-bus system, as shown in **Table 6**. Compared to scenario 1 of case 2, the suggested COA technique reduces the value of RPL from 325.74 kW to 305.58 kW, a reduction of 6.18%. In addition to this, the MVSI value is improved from 0.8375 to 0.8689, and the minimum bus voltage is increased from 0.9566 to 0.9655 p. u. According to Fig. 13, adding EVCS with DSTATCOM units has improved the VPs of the 136-bus RDN in comparison to case 1. Furthermore, the power loss in each branch is also reduced, as illustrated in Fig. 14.

4.3.3 Case 3

Similar to case 3 of the 33-bus RDN, the EVCS are optimally allocated in coordination with DG units by optimizing the MOF via COA under two distinct scenarios, WONR and WNR. In this case, the MOF considers both technical factors and economic factors.

A) Scenario 1 (WONR)

In this scenario, the impacts of EVCS' integration in coordination with DG units on various performance indices are studied for the 136-bus RDN. The potential bus locations for EVCSs are 90, 9, 82, 106, 131, and 49 on 136 bus RDN. The optimal size and site of DG units are presented in **Table 7**. The resulting values of IRPL, ITVD and MVSI are 0.3658, 0.6178 and 0.8714, respectively. The value of RPL and minimum bus voltage are 117.2 kW and 0.9662 p. u., respectively. In comparison to cases 1 and 2, integrating EVCS with DGs units significantly improved the voltage profile of the 136-bus network, as shown in Fig. 13. Furthermore, the power loss in each branch is reduced by integrating EVCS with DGs, as illustrated in Fig. 14. From the **Table 7**, it is noted that this scenario shows significantly higher improvements in terms of RPL reduction, voltage deviation reduction, and VSI maximization when compared to cases 1 and 2 of the 136-bus RDN.

B) Scenario 2 (WNR)

Similar to the 33-bus network, the integration of EVCSs with DGs and optimal NR resulted in a reduction in ITVD and IRPL while increasing VSI in the 136-bus network, as shown in **Table 7**. The potential bus locations for EVCS installation on the 136-bus RDN are 86, 92, 76, 18, 122, and 100. The opened switches for optimal NR and the location of DG units with their optimal sizes are also provided in **Table 7**. Compared to scenario 1 of case 2, the suggested COA technique reduces the value of RPL from 117.2 kW to 98.3 kW, a reduction of 16.12 %. In addition to this, the MVSI value is improved from 0.8714 to 0.9099, and the minimum bus voltage is increased from 0.9662 to 0.9766 p. u. The improved VP of each bus of the 136-bus network is shown in Fig. 13. Also, scenario 2 minimizes power loss at each of the branches of the 136-bus RDN, as illustrated in Fig. 14.

Table 7

Performances analysis of the 136-bus RDN with cases 3 and 4.

	Case 3		Case 4	
Scenario	WONR	WNR	WONR	WNR
Vmin (p. u.)/bus	0.9662/117	0.9766/117	0.9734/135	0.9797/97
IRPL	0.3658	0.3068	0.2638	0.2294
MVSI	0.8714	0.9099	0.8967	0.9202
ITVD	0.6178	0.5848	0.322	0.309
Total size of DG/DSTATCOM in [MW/MVAr]	11.641/---	12.151/---	11.5814/ 3.7947	11.720/ 3.884
RPL [kW]	117.2	98.3	84.5	73.5
EVs locations	90, 9, 82, 106, 131, 49	86, 92, 76, 18, 122, 100	19, 2, 64, 100, 40, 76	54, 86, 100, 64, 65, 76
DG sizes [MW]/ sites	2.7982(107), 1.3774 (91), 1.764 (53), 1.4625 (84), 2.0623 (32), 2.1762 (9)	2.310 (92), 1.450 (82), 2.359 (52), 2.185 (14), 2.176 (106), 1.671 (32)	2.015(14), 2.284(106), 1.13(93), 2.463(49), 1.294(84), 2.396(29)	1.148 (108), 2.9 (53), 1.285 (89), 1.337(106), 2.228 (74), 2.821 (39)
DSTATCOM sizes [MVAr]/ sites	---	---	0.735(32), 0.73(54), 0.437(95), 0.667(107), 0.515(16), 0.71(106)	0.6434 (14), 0.5279 (32), 1.0459 (26), 1.048 (136), 0.4983 (74), 0.120 (50)
Switches opened	S136-S156	S73, S137-S140-S142, S62, S144, S145, S134, S147-S152, S107, S126, S128, S156	S136-S156	S68, S9, S138, S27, S25, S141-S145, S83, S147-S152, S106, S126, S155, S156

4.3.4 Case 4

Similar to case 4 of the 33-bus RDN, the impacts of EVCS' integration in coordination with DG and DSTATCOM units on various performance indices are studied for the 136-bus RDN. The following are the two possible scenarios of this case:

A) Scenario 1 (WONR)

The potential bus locations for EVCS installation on the 136-bus RDN are 19, 30, 64, 100, 56, and 76. The optimal location of DG and DSTATCOM units, along with the optimal size are provided in **Table 7**. The resulting values of IRPL, ITVD, and MVSI are 0.2638, 0.3220, and 0.8967, respectively. Furthermore, the improved voltage profiles for each bus in this scenario are shown in Fig. 13, where bus 135 has a minimum voltage of 0.9734 p. u. Also, the active power loss in each branch is reduced due to the simultaneous integration of EVCS with DGs and DSTATCOMs units, as illustrated in Fig. 14.

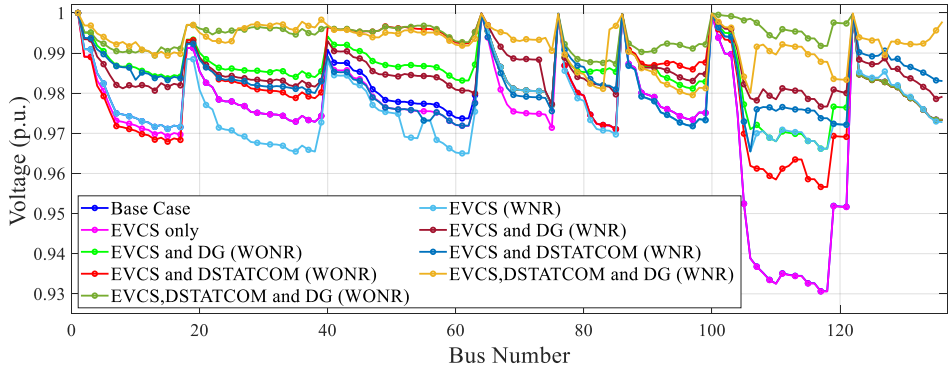

Fig. 13 – *Voltage profile of 136-bus RDN* (*Cases 1-4*).

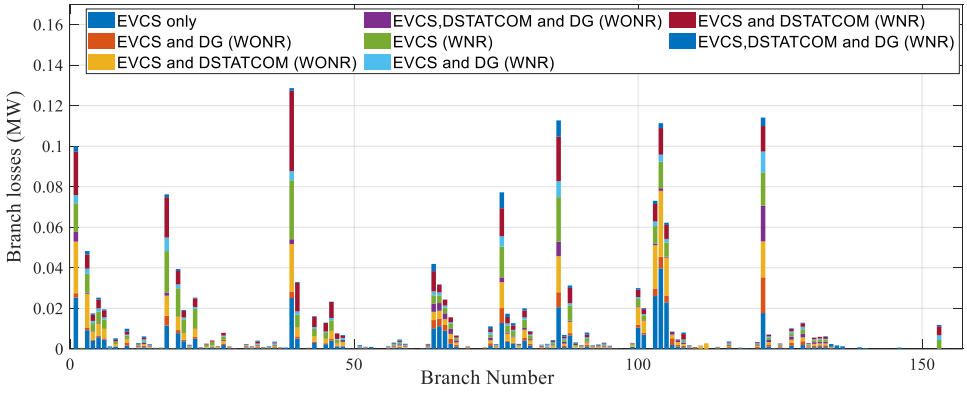

Fig. 14 – *Branch losses of 136-bus RDN* (*Cases 1-4*),

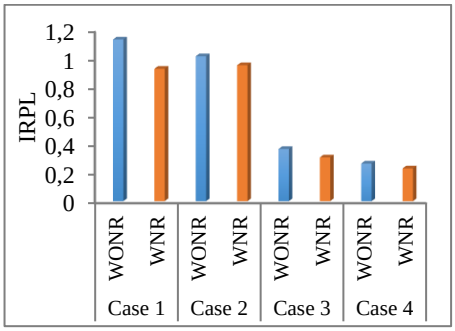

Fig. 15 – *IRPL for 136-bus RDN.*

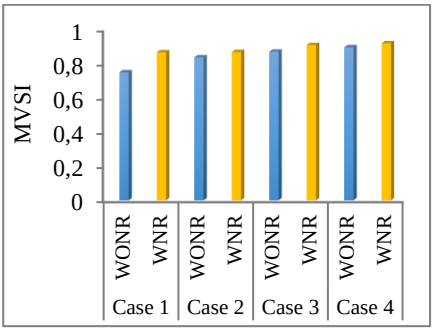

Fig. 16 – *VSI for 136-bus RDN.*

B) Scenario 2 (WNR)

The simultaneous optimal integration of EVCS, DG, and DSTATCOM units with NR has a higher impact on achieving the desired results of minimizing IRPL, ITVD, and VSI reduction on the 136-bus network, as shown in **Table 6**. Moreover, scenario 2 further lowers the IRPL value by 13.01 percent in comparison to WONR scenario. The minimum voltage is 0.9797 p. u. at bus 97, while the MVSI value is 0.9202. Also, the simultaneous integration of EVCS with DGs, DSTATCOMs and optimal NR significantly decreases power loss in each branch, as shown in Fig. 14. According to **Table 6**, the improvement in IRPL reduction, ITVD reduction, and VSI maximization is highest for scenario 2 of case 4 compared to other cases of the 136-bus network, as shown in Figs. 15 – 18. Furthermore, the scenario 2 of case 4 achieves a better VP when compared to other scenarios of the 136-bus RDN.

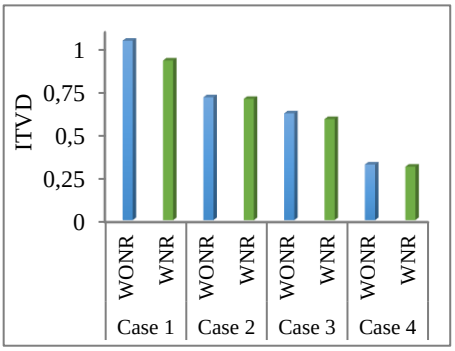

Fig. 17 – *ITVD for 136-bus RDN.*

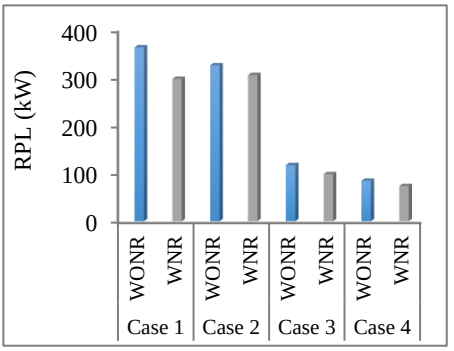

Fig. 18 – *RPL for 136-bus RDN.*

4.4 Comparisons of COA results from GWO and GA results

In this section, the results of COA are compared with the results of GWO [26] and the GA [27]. As the problem's complexity grows, it becomes more likely that the algorithm will get trapped at the local optimum value. In addition to this,

scenario 2 of case 4 is considered to assess the robustness of the COA for both the 33-bus and 136-bus RDNs. The dimension of the problem in scenario 2 of case 4 is 17 for 33-bus RDN (*i.e.*, 5 for NR, 6 for DSTATCOM sites and sizes, 6 for DG sites and sizes, and 3 for EVCS placement) and 51 for 136-bus RDN (*i.e.*, 21 for NR, 12 for DSTATCOM sites and sizes, 12 for DG sites and sizes, and 6 for EVCS placement). Each algorithm is run 25 times to assess the COA's effectiveness in solving optimization problems. To assess the robustness of COA, their performance characteristics are evaluated in terms of the best, mean, and worst values of objective functions, as illustrated in **Fig. 19.** The optimal solutions achieved by each technique for 33 bus and 136 bus networks are shown in **Table 8**. From Fig. 19 and **Table 8** it is observed that COA is a more reliable and effective approach than GWO and GA algorithms for solving complex optimization problems. Fig. 20 depicts the convergence curves of the best solution produced by adopted algorithms for scenario 2 of case 4 of the 136-bus RDN. In addition to this, it is seen that the COA exhibits a better convergence rate compared to GWO and GA.

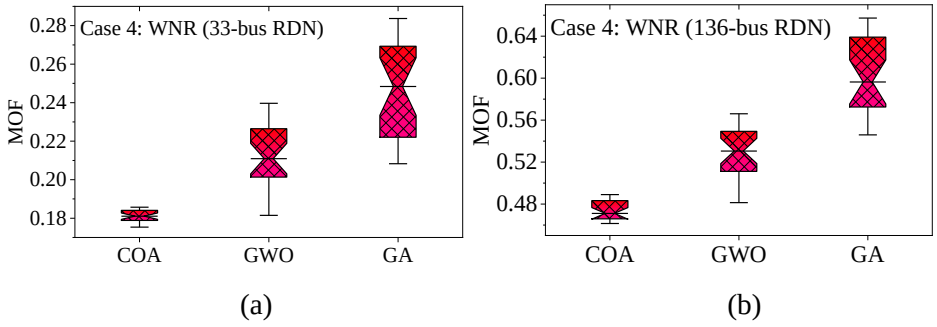

Fig. 19 – *Comparisons of COA from GWO and GA results.*

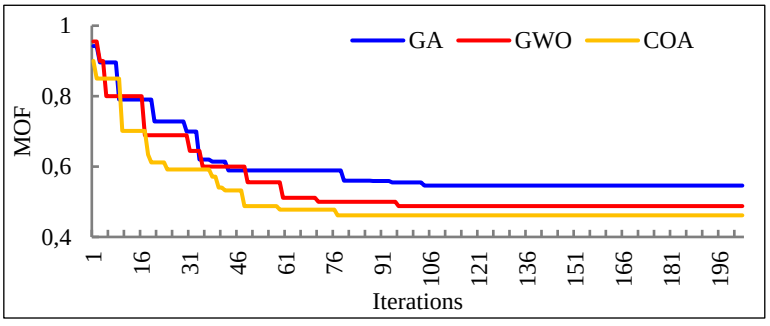

Fig. 20 – *Comparisons of convergence curve of COA from GWO and GA.*

Table 8

Comparison of COA performance for 33 and 136-bus RDNs (*Scenario 2 of case 4*).

System	Algorithm	Scenario	Switch opened	EVCS locations	DG sizes [MW]/sites	DSTATCOM sizes [MVAr]/sites	IRPL	ITVD	VSI	RPL [kW]
33-bus system	GA	WNR	S11, S7, S14, S31, S24	3, 19, 2	0.897/21, 0.811/18, 1.457/29	0.293/25, 0.339/21, 0.442/31	0.2083	0.1633	0.9425	43.96
	GWO	WNR	S11, S7, S14, S31, S25	3, 19, 2	0.888/21, 0.761/17, 1.541/29	0.367/25, 0.229/22, 0.525/30	0.1815	0.1912	0.9314	38.29
	COA	WNR	S11, S7, S34, S31, S24	3, 19, 2	1.03/21, 0.72/18, 1.41/29	0.29/25, 0.265/18, 0.51/30	0.1754	0.1424	0.9446	37.00
136-bus system	GA	WNR	S70, S137, S13, S38, S51, S141, S53, S62, S144, S90, S107, S126, S155, S156, S145-S151,	5, 65, 2, 71, 76, 122	2.209 (107), 1.259 (99), 3.00 (74), 1.861 (126), 2.254 (84), 1.464 (26)	0.307 (105), 0.413 (120), 1.035 (36), 0.739 (81), 0.644 (101), 0.619 (71)	0.3387	0.4264	0.9007	108.5
	GWO	WNR	S136-S139, S51, S94, S128, S141-S145, S80, S126, S147-S151, S105, S156	76, 64, 2, 100, 67, 40	2.404 (52), 1.507 (69), 1.507 (106), 1.992 (82), 2.404 (11), 2.308 (48)	0.72 (9), 0.661 (134), 0.45 (81), 0.7 (111), 0.701 (57), 0.546 (56)	0.2603	0.3412	0.9108	83.4
	COA	WNR	S68, S9, S138, S27, S25, S141-S145, S83, S147-S152, S126, S155,	54, 86, 100, 64, 65, 76	1.149 (108), 2.90 (53), 1.285 (89), 1.337 (106), 2.228 (74), 2.821 (39)	0.643 (14), 0.528 (32), 1.046 (26), 1.048 (136), 0.498 (74), 0.12 (50)	0.2294	0.3090	0.9202	73.5

5 Conclusions

Cleaner transportation may be possible with the advent of EVs. EVCSs are developed to promote the development of EVs. However, widespread EV adoption necessitates a robust and efficient charging infrastructure, which results in additional burden on the power distribution side. The objective of this research is to examine the impact of EVCS together with optimal NR and planning (siting and size) of DGs and DSTATCOMs on the RDN. The main goal is the maximization of technical and economic advantages of the system. Moreover, the results of COA are compared to the results of GWO and GA to evaluate its accuracy. Two distinct distribution systems have been subjected to four operating cases, including EVCSs, DGs, and DSTATCOMs. The impacts of EVCS deployment with DGs and DSTATCOM on RDN are also examined in two scenarios: WONR and WNR. The following is a summary of the key conclusions from the simulation:

– The integration of DG or DSTATCOM is advantageous in minimizing the detrimental impact of EVCS on power system performance. However, incorporating DG and DSTATCOM simultaneously with NR is a more efficient approach to reducing the negative impact of EVCS on the system performance.

– Significant improvements in IRPL reduction, ITVD reduction, and VSI enhancement are achieved when EVCS is optimally allocated together with DG

– and DSTATCOM, as well as with NR.

– Also, the simultaneous approach for optimal planning of EVCS, DG, and DSTATCOM with NR results in substantial technical and economic benefits.

– Better convergence characteristics of the COA have been found in comparison to the GWO and GA.

– The COA provides more accurate solutions compared to the GWO and GA.

6 References

[1] K. Balu, V. Mukherjee: Optimal Allocation of Electric Vehicle Charging Stations and Renewable Distributed Generation with Battery Energy Storage in Radial Distribution System Considering Time Sequence Characteristics of Generation and Load Demand, Journal of Energy Storage, Vol. 59, March 2023, p. 106533.

[2] J. S. Bhadoriya, A. R. Gupta, M. Zellagui, N. K. Saxena, A. K. Arya, A. K. Bohre: Optimal Allocation of Electric Vehicles Charging Station in Distribution Network Beside DG Using TSO, Ch. 29, Planning of Hybrid Renewable Energy Systems, Electric Vehicles and Microgrid, Springer, Singapore, 2022.

[3] M. Bilal, M. Rizwan, I. Alsaidan, F. M. Almasoudi: AI-Based Approach for Optimal Placement of EVCS and DG with Reliability Analysis, IEEE Access, Vol. 9, November 2021, pp. 154204 – 154224.

[4] M. S. Kumar Reddy, K. Selvajyothi: Optimal Placement of Electric Vehicle Charging Station for Unbalanced Radial Distribution Systems, Energy Sources, Part A: Recovery, Utilization, and Environmental Effects, February 2020, pp. 1 – 15.

[5] S. Pazouki, A. Mohsenzadeh, S. Ardalan, M.- R. Haghifam: Simultaneous Planning of PEV Charging Stations and DGs Considering Financial, Technical, and Environmental Effects, Canadian Journal of Electrical and Computer Engineering, Vol. 38, No. 3, Summer 2015, pp. 238 – 245.

[6] K. Kathiravan, P. N. Rajnarayanan: Application of AOA Algorithm for Optimal Placement of Electric Vehicle Charging Station to Minimize Line Losses, Electric Power Systems Research, Vol. 214, Part A, January 2023, p. 108868.

[7] V. K. B. Ponnam, K. Swarnasri: Multi-Objective Optimal Allocation of Electric Vehicle Charging Stations and Distributed Generators in Radial Distribution Systems Using Metaheuristic Optimization Algorithms, Engineering, Technology & Applied Science Research, Vol. 10, No. 3, June 2020, pp. 5837 – 5844.

[8] N. Dharavat, S. Kumar Sudabattula, V. Suresh: Optimal Integration of Distributed Generators (DGs) Shunt Capacitors (SCs) and Electric Vehicles (EVs) in a Distribution System (DS) using Marine Predator Algorithm, International Journal of Renewable Energy Research, Vol. 12, No. 3, September 2022, pp. 1637 – 1650.

[9] S. R. Gampa, K. Jasthi, P. Goli, D. Das, R. C. Bansal: Grasshopper Optimization Algorithm Based Two Stage Fuzzy Multiobjective Approach for Optimum Sizing and Placement of Distributed Generations, Shunt Capacitors and Electric Vehicle Charging Stations, Journal of Energy Storage, Vol. 27, February 2020, p. 101117.

[10] M. Bilal, M. Rizwan: Integration of Electric Vehicle Charging Stations and Capacitors in Distribution Systems with Vehicle-to-Grid Facility, Energy Sources, Part A: Recovery, Utilization, and Environmental Effects, May 2021, pp. 1 – 30

[11] A. Pratap, P. Tiwari, R. Maurya, B. Singh: Minimisation of Electric Vehicle Charging Stations Impact on Radial Distribution Networks by Optimal Allocation of DSTATCOM and DG Using African Vulture Optimisation Algorithm, International Journal of Ambient Energy, Vol. 43, No. 1, August 2022, pp. 8653 – 8672.

[12] K. E. Adetunji, I. W. Hofsajer, A. M. Abu-Mahfouz, L. Cheng: A Novel Dynamic Planning Mechanism for Allocating Electric Vehicle Charging Stations Considering Distributed Generation and Electronic Units, Energy Reports, Vol. 8, November 2022, pp. 14658 – 14672.

[13] A. Pratap, P. Tiwari, R. Maurya, B. Singh: A Novel Hybrid Optimization Approach for Optimal Allocation of Distributed Generation and Distribution Static Compensator with Network Reconfiguration in Consideration of Electric Vehicle Charging Station, Electric Power Components and Systems, Vol. 51, No. 13, April 2023, pp. 1302 – 327.

[14] M. S. Kumar Reddy, K. Selvajyothi: Investment Analysis for Optimal Planning of Electric Vehicle Charging Station on a Reconfigured Unbalanced Radial Distribution System, Electrical Engineering, Vol. 104, No. 3, June 2022, pp. 1725 – 1739.

[15] W. S. Tounsi Fokui, M. J. Saulo, L. Ngoo: Optimal Placement of Electric Vehicle Charging Stations in a Distribution Network with Randomly Distributed Rooftop Photovoltaic Systems, IEEE Access, Vol. 9, September 2021, pp. 132397 – 132411.

[16] S. Thumati, S. Vadivel, M. Venu Gopala Rao: Honey Badger Algorithm Based Network Reconfiguration and Integration of Renewable Distributed Generation for Electric Vehicles Load Penetration, International Journal of Intelligent Engineering and Systems, Vol. 15, No. 4, August 2022, pp. 329 – 338.

[17] M. Lavorato, J. F. Franco, M. J. Rider, R. Romero: Imposing Radiality Constraints in Distribution System Optimization Problems, IEEE Transactions on Power Systems, Vol. 27, No. 1, February 2012, pp. 172 – 180.

[18] R. S. Rao, K. Ravindra, K. Satish, S. V. L. Narasimham: Power Loss Minimization in Distribution System Using Network Reconfiguration in the Presence of Distributed Generation, IEEE Transactions on Power Systems, Vol. 28, No. 1, February 2013, pp. 317 – 325.

[19] A. Pahlavanhoseini, M. S. Sepasian: Scenario-Based Planning of Fast Charging Stations Considering Network Reconfiguration Using Cooperative Coevolutionary Approach, Journal of Energy Storage, Vol. 23, June 2019, pp. 544 – 557.

[20] D. Kothona, A. S. Bouhouras: A Two-Stage EV Charging Planning and Network Reconfiguration Methodology towards Power Loss Minimization in Low and Medium Voltage Distribution Networks, Energies, Vol. 15, No. 10, May 2022, p. 3808.

[21] S. Kaveripriya, V. Suresh, S. Suresh Kumar, K. Abinaya: Optimal Allocation of DERs in Distribution System in Presence of EVs, Proceedings of the 2nd International Conference on Power Engineering Computing and Control (PECCON), Chennai, India, December 2019, pp. 77 – 88.

[22] H. Tang, J. Wu: Multi-Objective Coordination Optimisation Method for DGs and EVs in Distribution Networks, Archives of Electrical Engineering, Vol. 68, No. 1, February 2019, pp. 15 – 32.

[23] S. R. Salkuti: Binary Bat Algorithm for Optimal Operation of Radial Distribution Networks, International Journal on Electrical Engineering and Informatics, Vol. 14, No. 1, March 2022, pp. 148 – 160.

[24] M. A. Akbari, M. Zare, R. Azizipanah-abarghooee, S. Mirjalili, M. Deriche: The Cheetah Optimizer: A Nature-Inspired Metaheuristic Algorithm for Large-Scale Optimization Problems, Scientific Reports, Vol. 12, No. 1, December 2022, p. 10953.

[25] J. R. S. Mantovani, F. Casari, R. A. Romero: Reconfiguracao de Sistemas de Distribuicao Radiais Utilizando o Criterio de Queda de Tensao, SBA Controle and Automacao, Vol. 11, No. 3, September 2000, pp. 150 – 159.

[26] S. Mirjalili, S. M. Mirjalili, A. Lewis: Grey Wolf Optimizer, Advances in Engineering Software, Vol. 69, March 2014, pp. 46 – 61.

[27] D. E. Goldberg, J. H. Holland: Genetic Algorithms and Machine Learning, Machine Learning, Vol. 3, No. 2-3, October 1988, pp. 95 – 99.

[28] S. Deb, K. Tammi, K. Kalita, P. Mahanta: Impact of Electric Vehicle Charging Station Load on Distribution Network, Energies, Vol. 11, No. 1, January 2018, p. 178.

[29] V. Janamala, U. Kamal Kumar, T. K. Sai Pandraju: Future Search Algorithm for Optimal Integration of Distributed Generation and Electric Vehicle Fleets in Radial Distribution Networks Considering Techno-Environmental Aspects, SN Applied Sciences, Vol. 3, March 2021, p. 464.

[30] T. T. Tran, K. H. Truong, D. N. Vo: Stochastic Fractal Search Algorithm for Reconfiguration of Distribution Networks with Distributed Generations, Ain Shams Engineering Journal, Vol. 11, No. 2, June 2020, pp. 389 – 407.

[31] S. Rao Gampa, D. Das: Optimum Placement and sizing of DGs Considering Average Hourly Variations of Load, International Journal of Electrical Power and Energy Systems, Vol. 66, March 2015, pp. 25 – 40.

[32] K. Balu, V. Mukherjee: Optimal Siting and Sizing of Distributed Generation in Radial Distribution System Using a Novel Student Psychology-Based Optimization Algorithm, Neural Computing and Applications, Vol. 33, No. 22, November 2021, pp. 15639 – 15667.

[33] K. R. Devabalaji, K. Ravi: Optimal Size and Siting of Multiple DG and DSTATCOM in Radial Distribution System Using Bacterial Foraging Optimization Algorithm, Ain Shams Engineering Journal, Vol. 7, No. 3, September 2016, pp. 959 – 971.

[34] A. Mohamed Imran, M. Kowsalya, D. P. Kothari: A Novel Integration Technique for Optimal Network Reconfiguration and Distributed Generation Placement in Power Distribution Networks, International Journal of Electrical Power & Energy Systems, Vol. 63, December 2014, pp. 461 – 472.

[35] M. Chakravorty, D. Das: Voltage Stability Analysis of Radial Distribution Networks, International Journal of Electrical Power & Energy Systems, Vol. 23, No. 2, February 2001, pp. 129-135.

[36] E. S. Oda, A. M. Abd El Hamed, A. Ali, A. A. Elbaset, M. Abd El Sattar, M. Ebeed: Stochastic Optimal Planning of Distribution System Considering Integrated Photovoltaic-Based DG and DSTATCOM Under Uncertainties of Loads and Solar Irradiance, IEEE Access, Vol. 9, February 2021, pp. 26541 – 26555.

[37] R. D. Zimmerman, C. E. Murillo-Sánchez, R. J. Thomas: MATPOWER: Steady-State Operations, Planning, and Analysis Tools for Power Systems Research and Education, IEEE Transactions on Power Systems, Vol. 26, No. 1, February 2011, pp. 12 – 19.

[38] M. A. Kashem, V. Ganapathy, G. B. Jasmon, M. I. Buhari: A Novel Method for Loss Minimization in Distribution Networks, Proceedings of the International Conference on Electric Utility Deregulation and Restructuring and Power Technologies, London, UK, April 2000, pp. 251 – 256.

[39] E. S. Oda, A. A. Abdelsalam, M. N. Abdel-Wahab, M. M. El-Saadawi: Distributed Generations Planning Using Flower Pollination Algorithm for Enhancing Distribution System Voltage Stability, Ain Shams Engineering Journal, Vol. 8, No. 4, December 2017, pp. 593 – 603.